GEOLOGICA CARPATHICA, 2025, 76, 4, 301–309 https://doi.org/10.31577/GeolCarp.2025.18

Different crystallization events of Li-bearing pegmatitic tourmaline from San Piero in Campo, Elba Island, Italy

ANDREAS ERTL[1,2,✉], FEDERICO PEZZOTTA[3], JOHN M. HUGHES[4], HANS-PETER MEYER[5], THOMAS LUDWIG[5], M. DARBY DYAR[6], GERALD GIESTER[2] and GEORGE R. ROSSMAN[7]

[1]Naturhistorisches Museum, Mineralogisch–Petrographische Abt., Burgring 7, 1010 Wien, Austria
[2]Universität Wien, Institut für Mineralogie und Kristallographie, Josef-Holaubek-Platz 2, 1090 Wien, Austria
[3]MUM – Mineralogical Museum "Luigi Celleri", Via Cavour 73, San Piero in Campo, Campo nell'Elba, 57034 (LI), Italy
[4]Department of Geology, University of Vermont, Burlington, Vermont 05405, U.S.A.
[5]Institut für Geowissenschaften, Universität Heidelberg, Im Neuenheimer Feld 234-236, 69120 Heidelberg, Germany
[6]Planetary Science Institute, 1700 East Fort Lowell, Tucson, Arizona 85719, U.S.A.
[7]Division of Geological and Planetary Sciences, California Institute of Technology, Pasadena, California 91125-2500, USA

(Manuscript received September 24, 2025; accepted in revised form October 31, 2025; Associate Editor: Pavel Uher)

Abstract: To learn more about the growth zones of distinctly zoned tourmalines from the well-studied Rosina aplite–pegmatite dike of the Monte Capanne pluton near San Piero in Campo, Elba Island, Italy, four tourmaline crystals rooted in the pegmatitic rock and developed into three different small cavities, as well as one additional crystal growing frozen in the pegmatitic rock, were chemically characterized. The light element contents and the unit cell parameters of the four samples were also determined. Black Fe^{2+}-rich tourmaline, grown directly within the pegmatite, with unit cell parameters a=15.97–15.98 Å, c=7.15–7.16 Å, can be assigned to schorl and fluor-schorl with only 4 % Fe^{3+}. The Fe content decreases during crystallization, whereas Mn and F contents increase (up to 8 wt% MnO and 1.4 wt% F), forming a growth sector of olive-green colour. Such olive-green tourmaline exhibits unit cell parameters of a=15.87–15.94 Å, c=7.12–7.14 Å and can be assigned to fluor-tsilaisite and Mn^{2+}-rich fluor-elbaite. Later, the Mn content decreases and the Al and Li contents increase (up to 44 wt% Al_2O_3 and 1.7 wt% Li_2O). These zones can have Ga and Pb contents of up to ~1100 and ~500 ppm, respectively. The colour of such tourmaline can be pale olive-green, pale pink, or colourless. These crystal zones have unit cell parameters of a=15.78–15.82 Å, c=7.08–7.10 Å, and can be assigned to fluor-elbaite, elbaite, rossmanite, and darrellhenryite. In the final stage of tourmaline crystallization, the F content in the investigated crystal terminations can drop down to 0.1 wt% F, while the (Fe+Mn) content increases. Usually, these terminations can be assigned to elbaite (a=15.79–15.83 Å, c=7.08–7.10 Å). When comparing the F content and the X-site charge (Na, Ca), all zones grown in the pegmatite pocket, except for the termination, show a strong positive correlation for each crystal examined. This observation is interpreted as evidence that the caps of the tourmaline crystals in the pegmatite pockets formed during a different event than the previously grown crystals.

Keywords: tourmaline, zonation, pegmatite pockets, crystallization events, Rosina aplite-pegmatite, Monte Capanne pluton

Introduction

The Rosina aplite–pegmatite dike (up to 2 m wide in the shallowest zone) of the Monte Capanne pluton near San Piero in Campo, Elba Island, Italy, has complex asymmetric zoning. It contains small to large pockets rich in accessory minerals, including a variety of multicoloured tourmalines (Pezzotta 1994, 2000, 2021; Pezzotta et al. 1996; Pezzotta & Orlandi 1998; Pezzotta & Guastoni 2007). A detailed description of the new tourmaline celleriite, as well as brief mentions of the tourmalines schorl, foitite, elbaite, fluor-elbaite, and rossmanite from this locality, was given by Bosi et al. (2022).

Tourmalines are complex aluminium-borosilicate minerals with strongly varying compositions related to isomorphous substitutions. The general formula of minerals of the tourmaline supergroup is $XY_3Z_6(BO_3)_3T_6O_{18}V_3W$ (details see Henry et al. 2011), with the most common site occupants:

X=Ca^{2+}, Na^{+}, K^{+}, □ (vacancy)
Y=Li^{+}, Mg^{2+}, Fe^{2+}, Mn^{2+}, Al^{3+}, Cr^{3+}, V^{3+}, Fe^{3+}, Mn^{3+}, Ti^{4+}
Z=Al^{3+}, Mg^{2+}, Fe^{3+}, V^{3+}, Cr^{3+}
T=Si^{4+}, Al^{3+}, B^{3+}
V=OH^{-}, O^{2-}
W=OH^{-}, F^{-}, O^{2-}.

Multicoloured tourmalines from the Elba Island often have darker-coloured terminations due to the incorporation of Fe and/or Mn. A tourmaline crystal found naturally broken into two fragments in a wide miarolitic cavity in the Rosina pegmatite (San Piero in Campo, Elba Island, Italy) and characterised by dark-coloured, late-stage overgrowths was recently studied by Altieri et al. (2023a).

Microstructural and paragenetic observations, together with compositional and spectroscopic data (electron microprobe

✉ corresponding author: Andreas Ertl
andreas.ertl@a1.net

and optical absorption spectroscopy), provide evidence that the formation of the dark-coloured and Mn-rich overgrowths could be the result of a partial re-opening of the geochemical system, possibly due to pocket rupture. Altieri et al. (2023a) argue that the tourmaline fragments were originally parts of a single crystal that underwent natural breakage followed by the simultaneous growth of Mn-rich dark terminations at both breakage surfaces, with slightly different compositions and with a significantly different growth rate at the analogous and antilogous poles. Further investigation by Altieri et al. (2023b) used chemistry and spectroscopy combined with structural and paragenetic observations of the cavities. That study proposes a detailed general genetic model in which, because of a pocket rupture event, chemical alteration of Fe- and Mn-rich minerals that formed early in the pegmatitic rock surrounding the cavities occurred through leaching processes, produced by the action of the highly reactive late-stage cavity fluids. Such processes could be responsible for the release of Fe and Mn in the geochemical system, allowing the formation of the late-stage dark-coloured terminations in the tourmaline crystals (Altieri et al. 2023b).

In this article, we examine various tourmaline samples, some of which have grown in small cavities and exhibit zonation, to decipher the nature of the chemical zonation and to assign the individual zones to members of the tourmaline supergroup. We then attempted to find further evidence that the late-stage terminations of the tourmaline crystals grew during a partial reopening of the geochemical system, possibly due to pocket rupture.

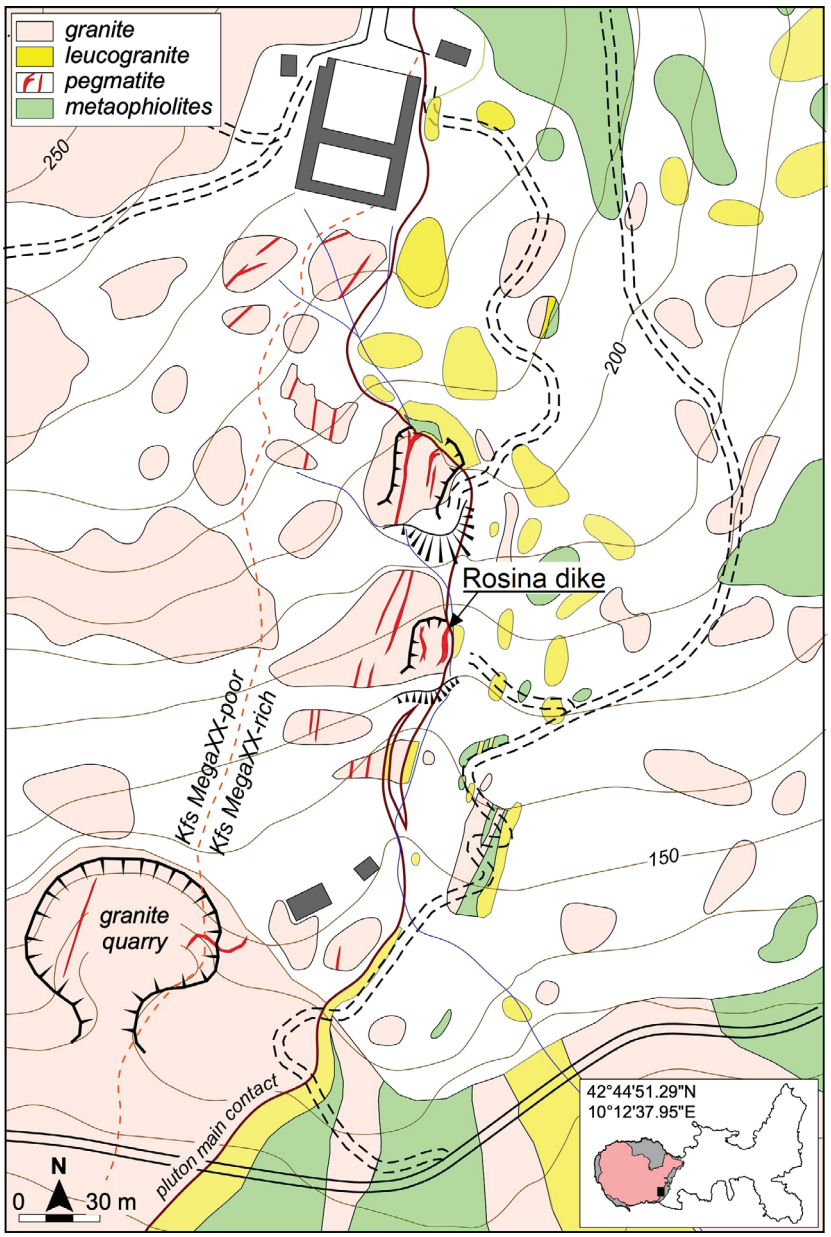

Fig. 1. Geological map of the Rosina pegmatite area, Elba Island, Italy. Elba Island is shown at the bottom right. The section of the geological map on Elba Island is marked by a black square. The exact coordinates of Rosina dike are also given.

Geological setting

Pegmatitic dikes occur along the eastern boundary of the Monte Capanne pluton (Fig. 1). This pluton, which covers the western side of the island, is a peraluminous biotite-monzogranite intrusion (Dini et al. 2002) formed by the upwelling of several magma pulses (Farina et al. 2010). After the formation of the main pluton, a series of miarolitic, Li-bearing aplite–pegmatite dikes were emplaced throughout the intrusion over an area of less than 4 km^2 along the eastern side of the monzogranite pluton of Monte Capanne (Marinelli 1959; Pezzotta 2000).

The aplitic–pegmatitic dikes of Monte Capanne (aged 6.7–6.9 million years) were classified by Pezzotta (2000) into four different groups based on their internal structures, mineralogy, and degree of geochemical evolution (Orlandi & Pezzotta 1996):

I. Dikes without Li minerals
II. Lithium-bearing dikes with complex asymmetric structural, mineralogical, and geochemical zoning
III. Lithium-bearing dikes with simple asymmetric structural, mineralogical, and geochemical zoning
IV. Irregularly zoned to unzoned Li-bearing dikes

The degree of geochemical fractionation increases from Group I to Group IV. The geochemically less developed dikes of Group I are predominantly located in the granitoids of the pluton, while the most developed dikes of Group IV are found in the contact metamorphic rocks (metasediments and metaserpentinites) of the aureole. The tourmaline crystals examined originate from the Rosina aplite-pegmatite (Fig. 1), a Group II pegmatite.

Analytical methods

Sample selection and radiation experiments

In this study, a group of tourmaline samples collected in a mining campaign in 2008 in the Rosina Pegmatite by A.E. and F.P. was examined. In particular, four tourmaline crystals rooted in the pegmatitic rock and developed into three different small cavities were characterized chemically, including light element analyses. Tourmaline #1 (Fig. 2) is a crystal with a length of ~3.5 cm and a diameter of ~8 mm, on a hand specimen, grown in a pocket. This crystal is composed of five zones, including the termination. All zones except the first one (grown in the pegmatite) developed into the pocket. The core of a black tourmaline with ~2.5 cm in diameter, grown frozen in the pegmatite, was also characterized (tourmaline #2). All zones (including the termination) were studied from a tourmaline crystal of ~4 cm length found in another pocket (tourmaline #3). In addition, two terminations of smaller tourmaline crystals with a length of ~5 mm from other small pockets were described. The termination of tourmaline #4 has a pale purple colour, whereas that of #5 was colourless. Additionally, two pale olive-green and two pale pink tourmaline crystals from other cavities, both with a length of ~1 cm, were used for the determination of some trace elements and for gamma irradiation with a ^{137}Cs source.

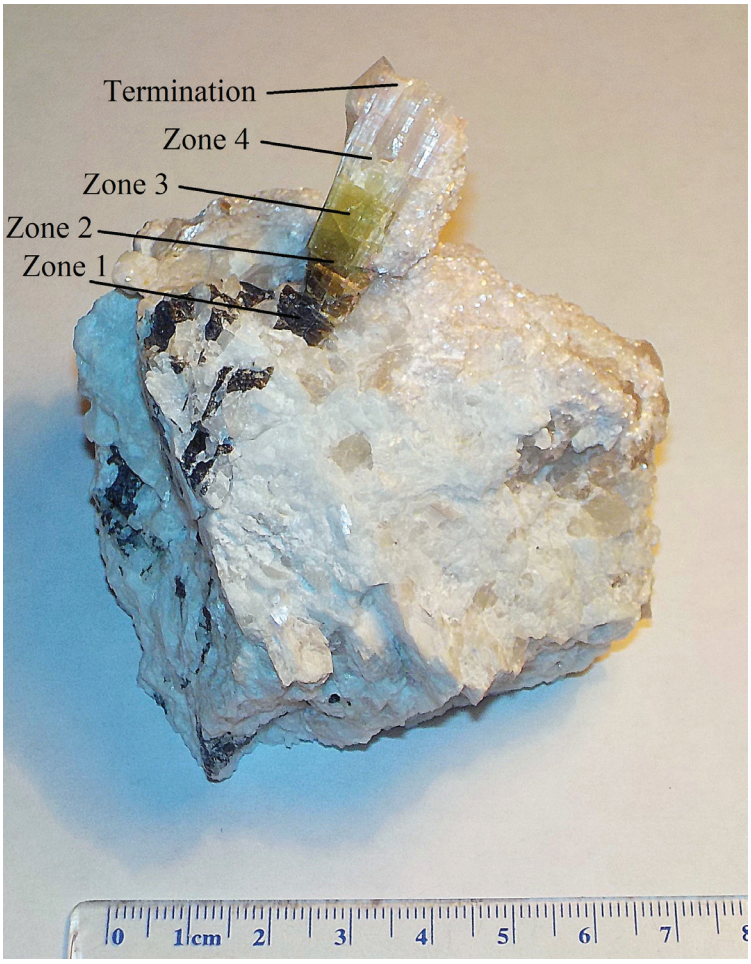

Fig. 2. Hand specimen with investigated zoned tourmaline #1 from Rosina dike, San Piero in Campo, Elba Island, Italy.

Unit cell parameter determination

Tourmaline samples #1 (all zones), #3 (zones 1, 2, termination), and #4 were measured at the University of Vermont on an Apex II CCD diffractometer from Bruker AXS equipped with a monocapillary optics collimator and graphite-monochromatized MoKα radiation. Tourmaline samples #2, #3 (zones 3, 4), and #5 were studied at the University of Vienna on a Bruker APEX II diffractometer equipped with a CCD area detector, and an Incoatec Microfocus Source IμS (30 W, multilayer mirror, MoKα). The refined unit cell parameters are listed in Table 1.

Chemical analysis

The crystal fragments used for the unit cell parameter determination were embedded in epoxy resin on a single round glass slide of 2.5 cm diameter and polished. All elements reported here, except B, Li, Be, and H, were determined with a Cameca SX50 electron probe microanalyser (EPMA) equipped with five wavelength-dispersive spectrometers (Universität Heidelberg). Operating conditions: 15 kV accelerating voltage, 20 nA beam current, and 5 μm beam diameter. Peaks for all elements were measured for 10 s, except for Mg (20 s), Ti (20 s), Zn (30 s), and F (40 s). Because the F Kα line interferes with the Fe- and MnLα lines, the measured F values require a correction, which is described in detail by Ertl et al. (2009). The following (natural and synthetic) reference materials and X-ray lines were used for calibration: topaz (F *K*α), albite (Na *K*α), wollastonite (Si *K*α) and (Ca *K*α), corundum (Al *K*α), periclase (Mg *K*α), orthoclase (K *K*α), rutile (Ti *K*α), rhodonite (Mn *K*α), hematite (Fe *K*α), and gahnite (Zn *K*α). Analytical data were reduced and corrected using the PAP routine (Pouchou & Pichoir 1991). A modified matrix

Table 1: Compositions and lattice parameters of tourmalines of the Rosina dike, San Piero in Campo, Campo nell'Elba, Livorno Province, Tuscany, Italy (wt%, standard deviation in parentheses).

	Tourmaline #1					Tourmaline #2	Tourmaline #3					Tourmaline #4	Tourmaline #5
	zone 1	zone 2	zone 3	zone 4	termination	core	zone 1	zone 2	zone 3	zone 4	termination	termination	termination
Sample	T1Z1	T1Z2	T1Z3	T1Z4	T1T	T2C	T3Z1	T3Z2	T3Z3	T3Z4	T3T	T4T	T5T
Colour	black	olive-green	pale olive-green	very pale green	pale pink	black	pale olive-green	pale pink	colourless	pale pink	very pale purple	pale purple	colourless
a [Å]	15.980(1)	15.947(1)	15.936(1)	15.851(1)	15.827(1)	15.968(1)	15.874(1)	15.806(1)	15.780(1)	15.819(1)	15.821(1)	15.832(1)	15.792(1)
c [Å]	7.160(1)	7.141(1)	7.137(1)	7.104(1)	7.096(1)	7.151(1)	7.121(1)	7.095	7.087(1)	7.100(1)	7.096(1)	7.104(1)	7.084(1)
SiO_2	34.46(34)	35.42(21)	36.09(30)	36.85(29)	36.40(23)	33.99(20)	36.52(27)	37.07(14)	36.61(17)	36.88(15)	36.90(22)	36.74(34)	35.31(16)
TiO_2	0.67(3)	0.45(6)	0.22(1)	0.09(2)	0.01(1)	0.87(4)	0.20(5)	0.01(1)	0.01(1)	0.01(1)	0.02(1)	0.02(1)	b.d.
B_2O_3[1]	10.27	10.15	10.29	11.57	12.12	10.32	10.21	12.40	12.60	12.19	12.05	12.07	13.05
B_2O_3[2]	10.12	10.40	10.53	11.57	12.01	10.05	10.58	12.00	12.35	12.19	11.98	11.92	12.58
Al_2O_3	33.29(11)	35.93(21)	37.39(13)	42.34(47)	43.49(19)	32.56(44)	37.82(6)	44.29(12)	44.59(20)	43.97(13)	43.21(11)	42.64(64)	43.99(22)
FeO_{total}	13.00(15)	3.15(10)	0.29(1)	b.d.	0.01(1)	14.54(20)	0.41(5)	0.02(1)	0.02(1)	0.01(1)	0.04(2)	0.24(7)	0.03(2)
FeO*	12.48	3.02	0.28	–	0.01	13.96	0.39	0.02	0.02	0.01	0.04	0.23	0.03
Fe_2O_3*	0.58	0.14	0.01	–	–	0.65	0.02	–	–	–	–	0.01	–
MnO	1.63(6)	6.48(23)	8.02(20)	1.41(38)	0.05(2)	0.65(5)	5.07(5)	0.13(3)	0.06(3)	0.04(2)	0.21(2)	1.06(40)	0.14(8)
MgO	0.04(1)	b.d.	b.d.	b.d.	b.d.	0.44(14)	b.d.	b.d.	b.d.	b.d.	b.d.	b.d.	b.d.
CaO	0.09(1)	0.16(2)	0.04(1)	0.34(4)	0.05(1)	0.21(3)	0.34(11)	0.07(1)	0.03(1)	0.02(1)	0.19(1)	0.01(1)	0.12(7)
Li_2O	0.17	0.69	0.69	1.72	1.71	0.06	1.20	1.24	1.19	1.45	1.73	1.16	1.18
ZnO	0.16(4)	0.20(4)	0.07(4)	0.01(1)	0.01(1)	0.09(3)	0.03(2)	0.02(2)	0.02(2)	0.01(1)	0.01(1)	0.02(2)	0.02(2)
Na_2O	1.90(3)	2.45(6)	2.11(5)	1.98(13)	1.94(2)	1.82(5)	2.49(6)	1.75(5)	1.64(4)	1.87(4)	1.85(4)	2.23(8)	2.20(9)
K_2O	0.04(2)	0.02(1)	0.02(1)	0.01(1)	0.01(1)	0.04(1)	0.01(1)	0.01(1)	0.01(1)	0.01(1)	0.01(1)	0.01(1)	0.01(1)
F	0.67(3)	1.43(10)	1.14(14)	1.23(6)	1.08(13)	0.59(7)	1.33(29)	0.53(2)	0.46(2)	0.57(13)	1.13(6)	0.24(14)	0.07(2)
H_2O[1]	2.79	2.69	2.83	2.70	2.63	2.77	2.62	2.81	2.74	2.59	2.59	2.82	2.75
H_2O3	2.90	2.69	2.83	3.10	3.20	2.94	2.74	3.08	3.21	3.21	3.20	3.48	3.40
O≡F	−0.28	−0.60	−0.48	−0.52	−0.45	−0.25	−0.56	−0.22	−0.19	−0.24	−0.48	−0.10	−0.03
Total	98.92	98.88	98.96	100.13	99.52	98.67	98.18	100.00	100.00	100.00	100.00	99.66	99.02

Note: T1Z1: Average of 11 EMPA data; T1Z2: Average of 20 EMPA data; T1Z3: Average of 15 EMPA data; T1Z4: Average of 8 EMPA data; T1T: Average of 14 EMPA data; T2C: Average of 10 EMPA data; T3Z1: Average of 20 EMPA data; T3Z2: Average of 18 EMPA data; T3Z3: Average of 9 EMPA data; T3Z4: Average of 13 EMPA data; T3T: Average of 15 EMPA data; T4T: Average of 15 EMPA data; T5T: Average of 13 EMPA data. All samples: H_2O, B_2O_3, Li_2O 1 SIMS analysis. [1] SIMS data. [2] Weight percent of B_2O_3 calculated for an optimized formula by considering the B_2O_3 SIMS values, the ∑(FeO+MnO), the cell volumes and by taking care that B≥3 apfu and that the formulae are charge balanced. The measured B_2O_3 SIMS values are within an error of 0-5 % in good agreement with the optimized B_2O_3 content. [3] Weight percent of H_2O calculated for an optimized formula by considering the H_2O SIMS values, a total sum close to 100 %, that $Y+Z+T\leq15.00$ apfu and that the formulae are charge balanced. The measured H_2O SIMS values are within an error of 0-19% in good agreement with the optimized H_2O content. The error increases when the sample contains less (FeO+MnO); b.d.: below detection limit. * FeO and Fe_2O_3 were recalculated by using Mössbauer spectroscopic data (Figs. 3 & 4).

correction was applied, assuming stoichiometric O atoms and all non-measured components as B_2O_3. The accuracy of the electron-microprobe analyses and the correction procedure were checked by measuring three samples of reference tourmalines (98114: elbaite, 108796: dravite, 112566: schorl). Compositions of these tourmaline samples were determined as part of an interlaboratory comparative study (Dyar et al. 1998, 2001). Under the described conditions, the accuracy of all analyses is ±1 % relative for major elements and ± 5 % relative for minor elements.

Hydrogen, Li, and B were determined by SIMS with a CAMECA IMS 3f ion microprobe (Universität Heidelberg). Primary O– ions were accelerated to 10 keV. The mass spectrometer's energy window width was 40 eV. An offset of 75 V was applied to the secondary accelerating voltage of 4.5 kV so that secondary ions with an initial energy of 75±20 eV were analyzed (energy filtering), which minimizes potential matrix effects (Ottolini et al. 1993). The primary current was 10 nA, resulting in a spot diameter of ~20 µm. The spectrometer's mass resolving power (MRP) M/ΔM for B, Li, and Si was set to ~1000 (10 %) to suppress interferences ($^6LiH^+$, $^{10}BH^+$, Al^{3+}). Secondary ^7Li, ^{11}B, and ^{30}Si ions were collected under an imaged field of 150 µm diameter. For H (and Si) the MRP M/ΔM was set to ~400 (10 %), and the imaged field was limited to a diameter of ~12 µm. In-situ water contamination was reduced by using a liquid nitrogen cold-trap attached to the sample chamber (Ludwig & Stalder 2007; and references therein). Count rates of the analysed isotopes (^1H, ^7Li, and ^{11}B) were normalized to the count rate of ^{30}Si, and relative ion yields (RIY) were used for quantification of the results (e.g., Hinton 1990, 1995; Ottolini et al. 1993). The RIY for H and B were determined using three tourmalines as reference material: elbaite, dravite, and schorl (Dyar et al. 1998, 2001). The reference material for Li and Be was the NIST SRM610 standard glass with concentrations for Li (464.2 µg g^{-1}) average taken from Pearce et al. (1997).

Relative reproducibility (1σ) for the RIY of H, Li, and B was <1 %. Matrix effects and the uncertainty of the element concentrations in the reference material limit the accuracy of the analysis. The relative accuracy is estimated to be <20 % for H and <10 % for Li and B. Table 1 contains complete chemical analyses of the studied crystal fragments of the Elba tourmalines.

Trace elements (Ga, Pb) were estimated by X-ray fluorescence (XRF) analyses of the samples performed with an INAM Expert 3L XRF unit with a Ti target using 60 s scans and standardless quantitative analyses with the INAM software (California Institute of Technology).

Mössbauer analysis

Mössbauer spectra were measured to determine the Fe^{3+} contents. Approximately 50 mg of each black Fe-rich tourmaline sample from the Rosina aplite-pegmatite dike was gently crushed under acetone, then mixed with a sugar-acetone solution designed to form sugar coatings around each grain and minimize preferred orientation. Grains were heaped in a sample holder confined by Kapton polyimide film tape. Spectra were measured at room temperature (295 K) using a source of 100–60 mCi ^{57}Co in Rh on a SEE Co. model WT302 spectrometer and corrected to remove the fraction of the baseline due to the Compton scattering of 122 keV gamma rays by electrons inside the detector. Details of the spectrum collection and analysis can be found in Dyar et al. (1998). Run times were 24 h, and spectra were collected in 2048 channels and corrected for nonlinearity. Errors are estimated at ±3 % for doublet areas, and ±0.02 mm/s for peak width, centroid shift, and quadrupole splitting.

Results and discussion

Zonation of tourmaline samples

Crystallization begins with Fe^{2+}-rich and Mn^{2+}-containing tourmaline in the pegmatitic rock surrounding the cavities. Both samples examined have a total amount of ca. 13–15 wt % FeO in this first zone (Table 1). Black, Fe^{2+}-rich tourmaline (grown directly within the pegmatite) with unit cell parameters a=15.97–15.98 Å, c=7.15–7.16 Å, can be assigned to schorl and fluor-schorl based on its chemical composition (Table 2). Mössbauer spectra of both samples were fit to four doublets (details see Figs. 3 and 4). The first one, with an isomer shift of 0.22–0.46 mm/s, represents Fe^{3+} in octahedral coordination. The other three are subcomponents of a distribution corresponding to Fe^{2+} at the *Y* site. Interestingly, the Fe^{3+} content of ~4 % is quite similar for all investigated Fe-bearing tourmaline samples from this locality (~4 % Fe^{3+} of a termination consisting of celleriite; Bosi et al. 2022). The errors of Fe^{3+} (%) contents of samples as measured by Mössbauer spectroscopy are generally cited as ~1–3 % absolute for tourmaline (e.g., Dyar et al. 1998). However, the present spectra are of extremely high quality as shown by the very small standard uncertainties (Figs. 1, 2) and the results for total ferric iron are strikingly consistent. Thus, we estimate that the % Fe^{3+} values in this study are more accurate than those used in the study by Dyar et al. (1998) and are probably within ~2 % accuracy.

Gamma irradiation of pale pink and pale olive-green tourmaline crystals, equivalent to ~10 million years in a Californian tourmaline-bearing pegmatite, resulted in a significantly stronger colouration of these tourmalines due to oxidation of Mn^{2+} (Rossman 1982). Pale pink tourmaline showed a dark reddish-brown colour after gamma irradiation, while previously pale olive-green tourmaline changed to an intense greenish-brown colour. An explanation that the pale pink colour of the natural (untreated) tourmaline sample from this locality is caused by minor amounts of oxidized Mn is thus consistent with the results of this radiation experiment and with the relatively young age of this pegmatite dike. Likewise, only a small percentage of the Fe is oxidized in the Fe-containing samples, as Mössbauer studies confirmed.

Table 2: Site assignments of tourmalines of the Rosina dike, San Piero in Campo, Campo nell'Elba, Livorno Province, Tuscany, Italy.

Sample	*X* site	*Y* site	*Z* site	*T* site	*W* site	Tourmaline
T1Z1	$Na_{0.63}\square_{0.34}Ca_{0.02}K_{0.01}$	$Fe^{2+}_{1.79}Al_{0.73}Mn^{2+}_{0.24}Li_{0.12}Ti_{0.09}Zn_{0.02}Mg_{0.01}$	$Al_{5.92}Fe^{3+}_{0.08}$	$Si_{5.92}Al_{0.08}$	$F_{0.36}(OH)_{0.33}O_{0.31}$	Fluor-schorl
T1Z2	$Na_{0.80}\square_{0.17}Ca_{0.03}$	$Al_{1.02}Mn^{2+}_{0.92}Li_{0.46}Fe^{2+}_{0.42}Ti_{0.06}Zn_{0.03}\square_{0.09}$	$Al_{5.98}Fe^{3+}_{0.02}$	$Si_{5.92}Al_{0.08}$	$F_{0.76}O_{0.24}$	Fluor-tsilaisite
T1Z3	$Na_{0.68}\square_{0.31}Ca_{0.01}$	$Al_{1.24}Mn^{2+}_{1.12}Li_{0.46}Fe^{2+}_{0.04}Ti_{0.03}Zn_{0.01}\square_{0.10}$	Al_6	$Si_{5.96}Al_{0.04}$	$F_{0.60}O_{0.28}(OH)_{0.12}$	Fluor-tsilaisite
T1Z4	$Na_{0.60}\square_{0.34}Ca_{0.06}$	$Al_{1.72}Li_{1.08}Mn^{2+}_{0.19}Ti_{0.01}$	Al_6	$Si_{5.78}B_{0.13}Al_{0.10}$	$F_{0.61}(OH)_{0.24}O_{0.15}$	Fluor-elbaite
T1T	$Na_{0.59}\square_{0.40}Ca_{0.01}$	$Al_{1.92}Li_{1.07}Mn^{2+}_{0.01}$	Al_6	$Si_{5.68}B_{0.24}Al_{0.08}$	$F_{0.53}(OH)_{0.33}O_{0.14}$	Fluor-elbaite
T2C	$Na_{0.61}\square_{0.34}Ca_{0.04}$	$Fe^{2+}_{2.02}Al_{0.61}Mg_{0.11}Ti_{0.11}Mn^{2+}_{0.10}Li_{0.04}Zn_{0.01}$	$Al_{5.92}Fe^{3+}_{0.08}$	$Si_{5.88}Al_{0.12}$	$(OH)_{0.39}F_{0.32}O_{0.29}$	Schorl
T3Z1	$Na_{0.79}\square_{0.15}Ca_{0.06}$	$Al_{1.33}Li_{0.79}Mn^{2+}_{0.71}Fe^{2+}_{0.05}Ti_{0.03}\square_{0.09}$	Al_6	$Si_{6.00}$	$F_{0.69}O_{0.31}$	Fluor-elbaite
T3Z2	$Na_{0.53}\square_{0.46}Ca_{0.01}$	$Al_{2.13}Li_{0.78}Mn^{2+}_{0.02}\square_{0.07}$	Al_6	$Si_{5.77}B_{0.23}$	$O_{0.54}F_{0.26}(OH)_{0.20}$	Darrellhenryite
T3Z3	$\square_{0.50}Na_{0.49}Ca_{0.01}$	$Al_{2.16}Li_{0.75}Mn^{2+}_{0.01}\square_{0.08}$	Al_6	$Si_{5.69}B_{0.31}$	$O_{0.45}(OH)_{0.32}F_{0.23}$	Rossmanite
T3Z4	$Na_{0.56}\square_{0.44}$	$Al_{2.05}Li_{0.91}Mn^{2+}_{0.01}\square_{0.03}$	Al_6	$Si_{5.73}B_{0.27}$	$O_{0.39}(OH)_{0.33}F_{0.28}$	Elbaite
T3T	$Na_{0.56}\square_{0.41}Ca_{0.03}$	$Al_{1.87}Li_{1.08}Mn^{2+}_{0.03}Fe^{2+}_{0.01}\square_{0.01}$	Al_6	$Si_{5.74}B_{0.21}Al_{0.05}$	$F_{0.55}(OH)_{0.32}O_{0.13}$	Fluor-elbaite
T4T	$Na_{0.68}\square_{0.32}$	$Al_{1.90}Li_{0.74}Mn^{2+}_{0.14}Fe^{2+}_{0.03}\square_{0.19}$	Al_6	$Si_{5.77}B_{0.23}$	$(OH)_{0.65}O_{0.23}F_{0.12}$	Elbaite
T5T	$Na_{0.67}\square_{0.31}Ca_{0.02}$	$Al_{2.11}Li_{0.75}Mn^{2+}_{0.02}\square_{0.12}$	Al_6	$Si_{5.55}B_{0.41}Al_{0.04}$	$(OH)_{0.57}O_{0.40}F_{0.03}$	Elbaite

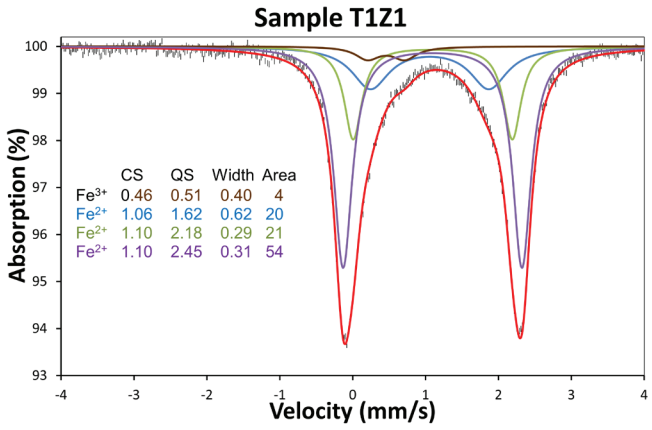

Fig. 3. Mössbauer spectrum of fluor-schorl from San Piero in Campo, Elba Island, Italy (tourmaline #1, zone 1). Results are given in mm/s relative to the center point of a Fe foil calibration spectrum. CS=centroid shift (in mms^{-1}) relative to α-Fe foil, QS = quadrupole splitting (in mms^{-1}), width=the Lorentzian peak-width at half-maximum (in mms^{-1}).

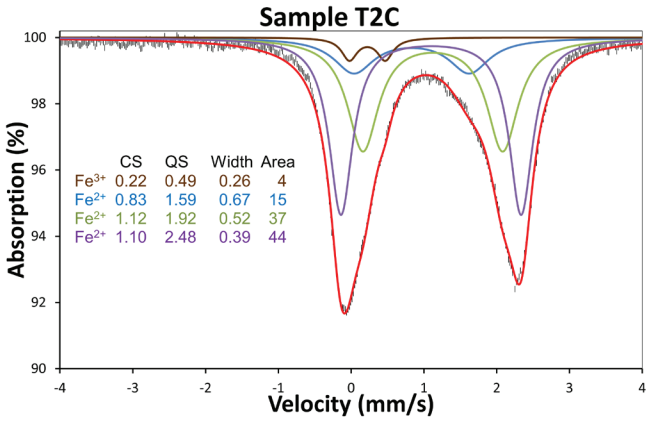

Fig. 4. Mössbauer spectrum of schorl from San Piero in Campo, Elba Island, Italy (tourmaline #2, core). Results are given in mm/s relative to the center point of a Fe foil calibration spectrum. CS=centroid shift (in mms^{-1}) relative to α-Fe foil, QS = quadrupole splitting (in mms^{-1}), width=the Lorentzian peak-width at half-maximum (in mms^{-1}).

During crystallization within the pockets, Fe content decreases while the Mn and F contents increase (up to 8 wt% MnO and 1.4 wt% F). These olive-green tourmaline zones exhibit unit cell parameters of a=15.87–15.95 Å, c=7.12–7.14 Å, and can be assigned to fluor-elbaite and fluor-tsilaisite.

In a later stage, Mn decreases while Al and Li contents increase (up to ~44 wt% Al_2O_3 and ~1.7 wt% Li_2O). Such tourmaline samples can be colourless or pale olive-green, pale pink, or pale purple. These zones show unit cell parameters of a=15.78–15.85 Å, c=7.09–7.10 Å, and consist of fluor-elbaite, elbaite, rossmanite, and darrellhenryite. Pale-coloured tourmaline samples (# GRR 3929) contain significant amounts of the trace elements Ga and Pb, as determined by XRF analyses. Pale olive-green tourmalines contain ~580–1050 ppm Ga and ~170–280 ppm Pb, while pale pink tourmalines contain ~580–1100 ppm Ga and ~70–500 ppm Pb.

At the slightly darker caps of both investigated zoned crystals, the FeO+MnO increases slightly. An even stronger increase in tourmaline terminations was already reported by Altieri et al. (2023a, b). The new Mn^{2+}-rich tourmaline end-member celleriite was also described from such tourmaline terminations by Bosi et al. (2022). In the final stage of tourmaline crystallization, F content drops to ≥0.1 wt%. The investigated tourmaline terminations exhibit unit cell parameters of a=15.79–15.83 Å, c=7.08–7.10 Å (Table 1) and can usually be assigned to elbaite, but also to fluor-elbaite (Table 2). The zones with the highest Al content contain significant amounts of $^{[4]}B$, equivalent to up to 20 mol% of ertlite, a B-rich tourmaline endmember with the formula $NaAl_3Al_6(Si_4B_2O_{18})(BO_3)_3(OH)_3O$ (Cempírek et al. 2025).

Correlations between tourmaline zones

A nearly ideal correlation (r^2=0.9993; y=0.784x+0.373) between fluorine content and *X*-site charge was reported in the study on the crystal growth of a zoned tourmaline

from a Li-rich pegmatite from the Himalaya Mine, San Diego co., California, USA (Ertl et al. 2010). This study also discusses a Ca-rich and Mg-bearing tourmaline that grew during the pocket's final crystallization stages and whose composition is outside such a correlation. As an explanation, Ertl et al. (2010) suggest an influence of the host rock on the growth of this late-stage crystal, affecting the composition of the late-stage fluids and creating a growth environment that differed from that of the first crystal formed in highly developed pegmatitic fractionated fluids.

Different multicolour tourmalines from the large gem-bearing pegmatite of Befisiotra, Madagascar, were chemically and structurally characterized by Ertl et al. (2021). A set of tourmaline samples (pink, green, yellowish, brown, black) from four different pockets found in this pegmatite was investigated. By plotting the fluorine content against the *X*-site charge, it was observed that these tourmaline samples plotted in two very high positive correlations with r^2=0.991 (ten samples) and r^2=0.992 (eight samples). These functions plot in a different field than the Himalaya Mine tourmalines and further have a higher slope. These two different correlations of the Befisiotra tourmalines were interpreted by these authors to indicate at least two different stages of crystallization within each pocket (Ertl et al. 2021).

These observed correlations were explained by a complex history of pocket crystallization within this relatively thick dike, resulting in complex compositional zoning of tourmaline crystals and possibly a multi-stage process of pocket evolution (Ertl et al. 2021).

When the fluorine contents of Rosina pegmatite crystals are plotted against the *X*-site charge for the first tourmaline (#1) examined, it can be seen that all zones grown in the pegmatitic pocket, except for the termination, show a positive correlation with r^2=0.9969 (y=1.038x+0.082; Fig. 5). Indeed, the tourmaline cap lies slightly outside of this linear function. Plotting the F content against the *X*-site charge of the second tourmaline crystal examined (#3), which was found in another pegmatite pocket, demonstrates that all zones, except for the termination, show a high positive correlation (r^2=0.9998, y=0.846x+0.326; Fig. 6). In this crystal, the cap also lies outside of this function, this time quite clearly. These observations are interpreted here as evidence that the caps of the tourmaline crystals in the Rosina pegmatite grew during a different event than the previously grown crystals.

Therefore, we agree with Altieri et al. (2023b) that the formation of the terminations of tourmaline crystals from the Rosina pegmatite can be associated with a dramatic physicochemical change in the crystallization environment due to an opening of the geochemical system. Furthermore, the model described by Altieri et al. (2023a) appears plausible, according to which the formation of the dark-coloured, Mn-rich overgrowths could be the result of pocket fracture.

The following crystallization sequence, including celleriite, was given by Bosi et al. (2022) for a tourmaline crystal from the Rosina dike: elbaite → fluor-elbaite → celleriite → rossmanite → celleriite. In other samples Altieri et al. (2023b) could observe this crystallization sequence for other samples: primary schorl → fluor-elbaite → elbaite (termination) and schorl → elbaite → elbaite (termination). As the final stage of overgrowth, Altieri et al. (2023a) described Mn-rich fluor-elbaite and elbaite. Recently, these crystallization sequences were reported: elbaite → fluor-elbaite → (Fe,Mg)-bearing darrellhenryite, elbaite → (Fe,Mg)-bearing darrellhenryite → schorl/foitite (Andreozzi et al. 2025) and Mn-rich schorl →

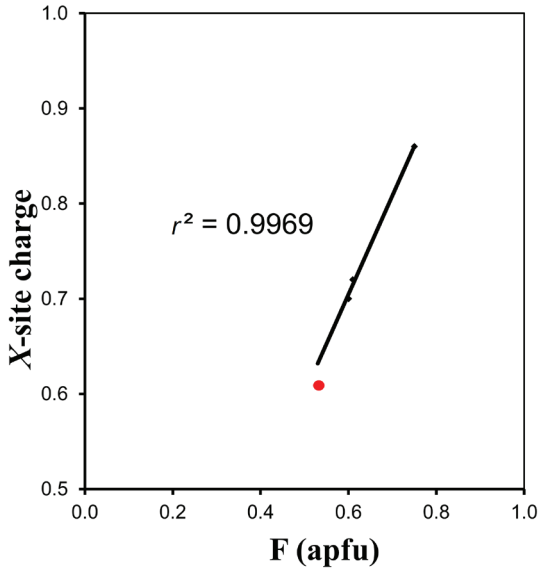

Fig. 5. Fluorine to *X*-site charge correlation of tourmaline #1 zones. All investigated zones grown in the pegmatitic pocket are plotted. The red filled circle represents the termination of this tourmaline crystal.

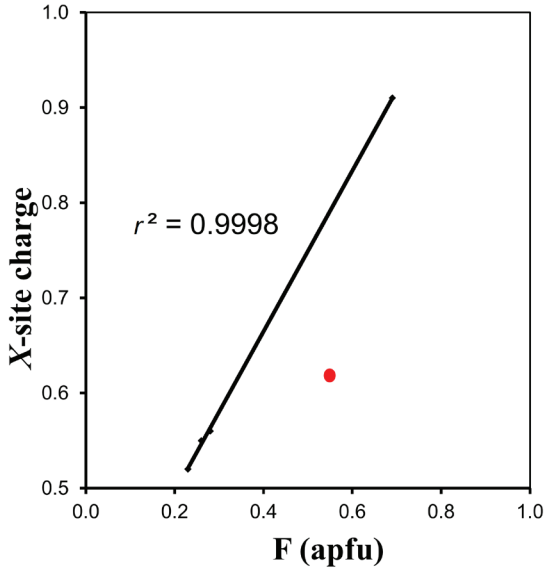

Fig. 6. Fluorine to *X*-site charge correlation of tourmaline #3 zones. All investigated zones grown in the pegmatitic pocket are plotted. The red filled circle represents the termination of this tourmaline crystal.

elbaite (Bosi et al. 2025). In our investigated samples we observed the following crystallization sequences: primary schorl/fluor-schorl → fluor-tsilaisite → fluor-elbaite → fluor-elbaite (termination) and fluor-elbaite → darrellhenryite → rossmanite → elbaite → fluor-elbaite (termination). In addition, terminations consisting of elbaite were identified.

Thus, primary schorl, as well as fluor-elbaite, elbaite, rossmanite, and darrellhenryite were confirmed. While we could not observe celleriite, schorl, or foitite as the final stage of overgrowth in our samples, we could confirm elbaite and fluor-elbaite. New, but not surprising, primary fluor-schorl as well as zones consisting of fluor-tsilaisite were verified for the first time. In contrast to the darrellhenryite described by Andreozzi et al. (2025), our sample does not contain significant amounts of Fe and Mg. Interestingly, compared to the neotype material elbaite from the Rosina pegmatite described by Bosi et al. (2025), our samples show that the chemical composition of elbaite from the Rosina pegmatite can be even poorer in F and more enriched in tetrahedrally coordinated B.

Conclusion

This work addressed the question of whether the caps of the tourmaline crystals in the pegmatite pockets formed during a different event than the previously grown crystals. Based on observed unit cell parameters and the chemical composition of the different tourmaline zones, it was found that after the crystal growth of primary Fe^{2+}-rich tourmaline (schorl, fluor-schorl), grown directly within the pegmatite, the Fe content decreases, while Mn^{2+} and F contents increase. This results in the formation of fluor-tsilaisite and Mn^{2+}-rich fluor-elbaite, respectively. Later, the Mn content decreases and the Al and Li contents increase, leading to the formation of fluor-elbaite, elbaite, rossmanite, and darrellhenryite. In the final stage of tourmaline crystallization, the F content in the investigated crystal terminations can drop significantly, while the (Fe+Mn) content increases. These terminations are usually classified as elbaite.

Based on the relationships between fluorine content and charge at the *X* site (Na, Ca), all tourmaline zones grown in the pegmatite pocket, except for the termination, show strong positive linear correlations. This observation is interpreted as evidence that the caps of the tourmaline crystals in the pegmatite pockets formed during a different event than the previously grown crystals. It is quite possible that tourmaline crystals that grew in pockets of other pegmatites also formed differently coloured caps during a further crystallization event, probably at a lower temperature than the other part of the crystal.

It is also interesting that individual zones of these investigated tourmaline crystals can have Ga and Pb contents of up to ~1100 and ~500 ppm, respectively. However, it is known that in rare cases Ga can be concentrated in Li-rich pegmatites.

Acknowledgements: We dedicate this publication to Igor Broska for his friendship, his enthusiasm and his continued scientific interest. This research was funded in part (AE) by the Austrian Science Fund (FWF) project P 35585. The Mössbauer spectrometer has now been relocated to the Department of Chemistry at the University of Idaho in the laboratory of Dr. Sebastien Stoian, who was gracious enough to run these samples for us. We thank Andreas Wagner, Vienna, Austria, for sample preparation work. Many thanks to Andrea Dini for helping with the creation of the geological map. We sincerely thank Peter Bačík, Jan Cempírek, and Pavel Uher for their careful reviews of the manuscript. For the purpose of open access, the author has applied a CC BY public copyright license to any Author Accepted Manuscript version arising from this submission.

References

Altieri A., Pezzotta F., Skogby H., Hålenius U. & Bosi F. 2023a: Dark-coloured Mn-rich overgrowths in an elbaitic tourmaline crystal from the Rosina pegmatite, San Piero in Campo, Elba Island, Italy: witness of late-stage opening of the geochemical system. *Mineralogical Magazine* 87, 130–142. https://doi.org/10.1180/mgm.2022.125

Altieri A., Pezzotta F., Andreozzi G.B., Skogby H. & Bosi F. 2023b: Genetic model for the color anomalies at the termination of pegmatitic gem tourmaline crystals from the island of Elba, Italy. *European Journal of Mineralogy* 35, 755–771. https://doi.org/10.5194/ejm-35-755-2023

Andreozzi G.B., Di Giuseppe D., Gualtieri A.F., Scognamiglio V., Fornasini L., Bersani D., Giovanardi T., Lugli F & Pezzotta F. 2025: Fibrous tourmaline from San Piero in Campo (Elba, Italy). *European Journal of Mineralogy* 37, 437–453. https://doi.org/10.5194/ejm-37-437-2025

Bosi F., Pezzotta F., Altieri A., Andreozzi G.B., Ballirano P., Tempesta G., Cempírek J., Škoda R., Filip J., Čopjaková R., Novák M., Kampf A.R., Scribner E.D., Groat L.A. & Evans R.J. 2022: Celleriite, $(Mn^{2+}{}_2Al)Al_6(Si_6O_{18})(BO_3)_3(OH)_3(OH)$, a new mineral species of the tourmaline supergroup. *American Mineralogist* 107, 31–42. https://doi.org/10.2138/am-2021-7818

Bosi F., Pezzotta F., Skobgy H., Luppi R., Ballirano P., Hålenius U., Tempesta G., Agrosì G. & Sejkora J. 2025: Elbaite, the neotype material from the Rosina pegmatite, San Piero in Campo, Elba island, Italy. *European Journal of Mineralogy* 37, 505–516. https://doi.org/10.5194/ejm-37-505-2025

Cempírek J., Jonsson E., Skřápková L., Škoda R., Kolitsch U., Čopjaková R., Groat L.A., Kampf A.R., Lussier A.J., Hawthorne F.C., Haifler J., Holá M. & Ende M. 2025: Ertlite, $NaAl_3Al_6(Si_4B_2O_{18})(BO_3)_3(OH)_3O$, a new mineral species of the tourmaline supergroup. *American Mineralogist* 110. https://doi.org/10.2138/am-2025-9816

Dini A., Innocenti F., Rocchi S., Tonarini S. & Westerman D.S. 2002: Magmatic evolution of the laccolith-pluton-dyke complex of Elba Island, Italy. *Geological Magazine* 139, 257–279. https://doi.org/10.1017/S0016756802006556

Dyar M.D., Taylor M.E., Lutz T.M., Francis C.A., Guidotti C.V. & Wise M. 1998: Inclusive chemical characterization of tourmaline: Mössbauer study of Fe valence and site occupancy. *American Mineralogist* 83, 848–864. https://doi.org/10.2138/am-1998-7-817

Dyar M.D., Wiedenbeck M., Robertson D., Cross L.R., Delaney J.S., Ferguson K., Francis C.A., Grew E.S., Guidotti C.V., Hervig R.L., Hughes J.M., Husler J., Leeman W., McGuire A.V., Rhede D., Rothe H., Paul R.L. & Richards I. 2001: Reference minerals for the microanalysis of light elements. *Geostandards Newsletter* 25, 441–463. https://doi.org/10.1111/j.1751-908X.2001.tb00616.x

Ertl A., Kolitsch U., Meyer H.-P., Ludwig T., Lengauer C.L., Nasdala L. & Tillmanns E. 2009: Substitution mechanism in tourmalines of the ''fluor-elbaite''-rossmanite series from Wolkenburg, Saxony, Germany. *Neues Jahrbuch für Mineralogie Abhandlungen* 186, 51–61. https://doi.org/10.1127/0077-7757/2009/0136

Ertl A., Rossman G.R., Hughes J.M., London D., Wang Y., O'Leary J.A., Dyar M.D., Prowatke, S., Ludwig T. & Tillmanns E. 2010: Tourmaline of the elbaite-schorl series from the Himalaya Mine, Mesa Grande, California: A detailed investigation. *American Mineralogist* 95, 24–40. https://doi.org/10.2138/am.2010.3271

Ertl A., Pezzotta F., Topa D. & Giester G. 2021: Multicolor tourmalines from pockets of the Befisiotra pegmatite Fianarantsoa Province, Madagascar: Indication of two different crystallization stages. In: EMPG – XVII, 17th International Symposium on Experimental Mineralogy, Petrology and Geochemistry, March 1–3, Conference Abstracts, 73.

Farina F., Dini A., Innocenti F., Rocchi S. & Westerman D.S. 2010: Rapid incremental assembly of the Monte Capanne pluton (Elba Island, Tuscany) by downward stacking of magma sheets. *Geological Society of America Bulletin* 120, 1463–1479. https://doi.org/10.1130/B30112.1

Henry D.J., Novák M., Hawthorne F.C., Ertl A., Dutrow B.L., Uher P. & Pezzotta F. 2011: Nomenclature of the tourmaline-supergroup minerals. *American Mineralogist* 96, 895–913. https://doi.org/10.2138/am.2011.3636

Hinton R.W. 1990: Ion microprobe trace-element analysis of silicates: Measurement of multi-element glasses. *Chemical Geology* 83, 11–25. https://doi.org/10.1016/0009-2541(90)90136-U

Hinton R.W. 1995: Ion microprobe analysis in geology. In: Potts P.J., Bowles J.F.W., Reed S.J.B. & Cave R.M. (Eds.): Microprobe Techniques in the Earth Sciences. *Cambridge University Press*, 235–289. https://doi.org/10.1007/978-1-4615-2053-5_6

Ludwig T. & Stalder R. 2007: A new method to eliminate the influence of in situ contamination in SIMS analysis of hydrogen. *Journal of Analytical Atomic Spectrometry* 22, 1415–1419. https://doi.org/10.1039/b705848a

Marinelli G. 1959: Le intrusioni terziarie dell'Isola d'Elba, Atti Società Toscana. *Scienze Naturali* 66, 50–253.

Orlandi P. & Pezzotta F. 1996: Minerali dell'Isola d'Elba, i minerali dei giacimenti metalliferi dell'Elba orientale e delle pegmatiti del M.te Capanne. *Ed. Novecento Grafico*, Bergamo, 1–248.

Ottolini I., Bottazzi P. & Vannucci R. 1993: Quantification of lithium, beryllium, and boron in silicates by secondary ion mass spectrometry using conventional energy filtering. *Analytical Chemistry* 65, 1960–1968. https://doi.org/10.1021/ac00063a007

Pearce N.J.G., Perkins W.T., Westgate J.A., Gorton M.P., Jackson S.E., Neal C.R. & Chenery S.P. 1997: A compilation of new and published major and trace element data for NIST SRM 610 and SRM 612 partially certified glass reference materials. *Geostandards and Geoanalytical Research* 21, 115–144. https://doi.org/10.1111/j.1751-908X.1997.tb00538.x

Pezzotta F. 1994: Helvite of a M.te Capanne pluton pegmatite (Elba Island, Italy): chemical, X-ray diffraction data and description of the occurrence. *Atti dell'Accademia nazionale dei Lincei. Rendiconti* 9, 355–362. https://doi.org/10.1007/BF03001653

Pezzotta F. 2000: Internal structures, parageneses and classification of the miarolitic Li-bearing complex pegmatites of Elba Island (Italy). In: Mineralogy and petrology of shallow depth pegmatites, Papers from the First International Workshop. *Memorie della Società Italiana di Scienze Naturali e del Museo Civico di Storia Naturale di Milano* 30, 29–43.

Pezzotta F. 2021: A history of tourmaline from the Island of Elba. *The Mineralogical Record* 52, 1–52.

Pezzotta F. & Guastoni A. 2007: Hambergite, helvite e pirofanite nelle pegmatiti elbane. *Rivista Mineralogica Italiana* 3, 166–168.

Pezzotta F. & Orlandi P. 1998: Découvertes minéralogiques récentes dans les pegmatites de l'île d'Elbe. *Le Règne Minéral* 4, Les Éditions du Piat, 31–38.

Pezzotta F., Hawthorne F.C., Cooper M.A. & Teertstra D.K. 1996: Fibrous foitite from San Piero in Campo, Elba, Italy. *Canadian Mineralogist* 34, 741–744.

Pouchou J.L. & Pichoir F. 1985: "PAP" $\phi(\rho z)$ correction procedure for improved quantitative microanalysis. In: Armstrong J.T. (Ed.): Microbeam analysis. *San Francisco Press*, San Francisco, 104–106.

Rossman G.R. 1982: Irradiation of colored gem stones. *International Geological Symposium, Proceedings* 1, 91–99.